Journal of Social Sciences and Technical Education, 3(1), 180-197
http://myjms.mohe.gov.my/index.php/jossted

Performance Analysis of the Rhombic Drive Beta-Configuration Stirling Engine

(Analisis Prestasi Enjin Stirling Konfigurasi Beta Rhombic Drive)

*JACKLY MURIBAN[1], ROSLI ABU BAKAR[2],
Refrigeration and Air Conditioning Department, Kolej Komuniti Kota Marudu, Malaysia[1]
Faculty of Mechanical & Automotive Engineering Technology, Universiti Malaysia Pahang, Malaysia[2]

* Corresponding author: jackly@kkkotamarudu.edu.my

ARTICLE INFO

Article History:
Received 30.06.2023
Accepted 08.08.2023
Published 23.11.2023

Abstract

Stirling Engines have a wide range of practical uses, including propulsion and refrigeration. The Stirling cycle heat motor has a decent potential for use in the future given certain benefits like external combustion, fuel adaptability and flexibility. Stirling engines are used extensively in the cryogenic and submarines field, but prime mover applications are still underdeveloped. The main purpose of this study is to develop accurate thermodynamic numerical models that can predict performance and provide a means of further optimization. Therefore, this paper shows numerical modelling simulation, validation, and parametric optimization of a Single-Cylinder Rhombic Drive Beta-Configuration Stirling Engine filled with CuO-ZnO as a working fluid. A general 1st Order-Dimensional numerical model is adapted throughout the prediction of Stirling engine performance. The numerical model is determined based on swept and un-swept volume, overall geometrical parameters, and operating fluid properties The cycle pressure, volumetric displacement, work, and energy produced during the expansion and compression cycles in the cylinder are predicted using Schmidt and Ideal Adiabatic analysis based on Berchowitz and Urieli's technique. At a speed of 300 rpm, the engine produces 946.54 W of power in the designated working condition. Based on a 90° phase angle setting, 4.5 bar of Copper Oxide-Zinc Oxide (CuO-ZnO) cylinder charge pressure, 1073 K of expansion space temperature, and 294 K of cooler space temperature, the stated thermal efficiency is 73 percent.

Keywords: Thermodynamic cycle, Beta-configuration, Nanoparticles, Numerical

INTRODUCTION

Manufacturers and Research & development are keen to create and improve power generator technology nowadays in order to provide a better environment. The present development is attributed to the emissions created by conventional power generators, which are causing more serious environmental issues (Chen et al., 2012). The continual burning of fuels from any fossil fuel-based energy conversion device has a negative influence on the environment and population inside the energy conversion system. Furthermore, the emissions created by fossil-fuel-based energy conversion equipment greatly raised the world emission level (Sripakagorn & Srikam, 2011).

An external combustion engine is a sort of energy conversion technology that differs from the principles of internal combustion engines. The external combustion engine does not require any internal combustion fuel propulsion, which gives a considerable benefit in terms of creating minimal emissions (Tlili et al., 2008). To create mechanical energy, the external combustion engine solely utilizes an external heat source. Because the external combustion engine is heated from the outside, any combustible substance may be utilized as fuel to continually supply heat and create power.

Stirling engines (SE) are one type of externally heated energy conversion technology that employs an external heat source to generate mechanical energy. Due to the absence of an internal combustion process, the Stirling engine has substantial benefits in terms of design and construction (Kongtragool & Wongwises, 2003). Besides, the Stirling engine's capacity to employ many types of heat sources (e.g., hot air) with minimal emissions levels positions it as one of the alternative methods of minimizing environmental concerns for green energy generation (Thombare & Verma, 2008).

In the present work, the thermodynamic numerical models are conducted that can predict performance and provide a means of further optimization of the Stirling Engine. Therefore, this paper shows numerical modelling simulation, validation, and parametric optimization of a Single-Cylinder Rhombic Drive Beta-Configuration Stirling Engine filled with CuO-ZnO as a working fluid.

METHODOLOGY

The simulation model of this rhombic drive beta-configuration Stirling engine is continuity with the previous research by (Farid et al., 2019), and the thermodynamic prediction is carried out based on the methodology employed which was originally developed by (Urieli & Berchowitz, 1984). Based on the methodology presented, a revised and simplified Stirling Engine Analysis (SEA) MATLAB is developed, as shown in Figure 1.

The Schmidt analysis is used to initialize the ideal adiabatic condition for prediction. In this study, a similar methodological approach is used for the engine's working environment. It is assumed that there are no internal heat exchanger surfaces and that the heat addition and rejection process is solely dependent on the displacer and power piston cylinder walls. Figure 2, depicts a schematic of rhombic drive BCSE. The working area is divided into three sections: the hot-end expansion space, the regenerator space, and the compression space (cold-end). The expansion space changes as the displacer piston move through a cycle. Meanwhile, the compression area varies as a result of both the displacer and power pistons moving. Two spur gear units of identical radius mesh rotate in opposite directions. Four identical connecting rod components, the displacer piston, and the power piston yoke are used to provide reciprocating motion without side thrust for both the displacer piston and the power piston. In reference to the vertical center line, the entire pattern is symmetrical. The total rhombic drive geometrical properties of beta configuration engine components Table 1. shows Stirling engines that use rhombic driving principles with adjustments for engine stroke, phase angle, compactness, component tolerance, and failure factors.

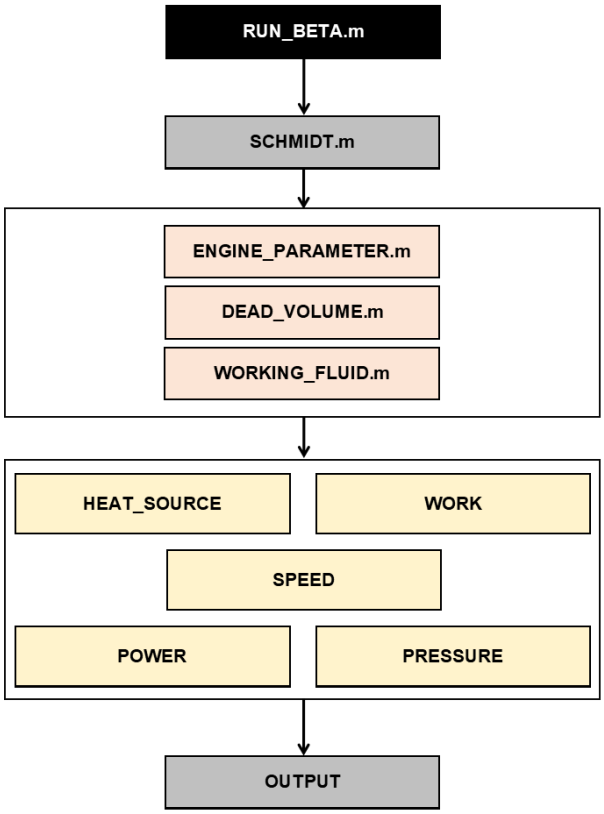

Figure 1. Simplified Simulation Program Layout

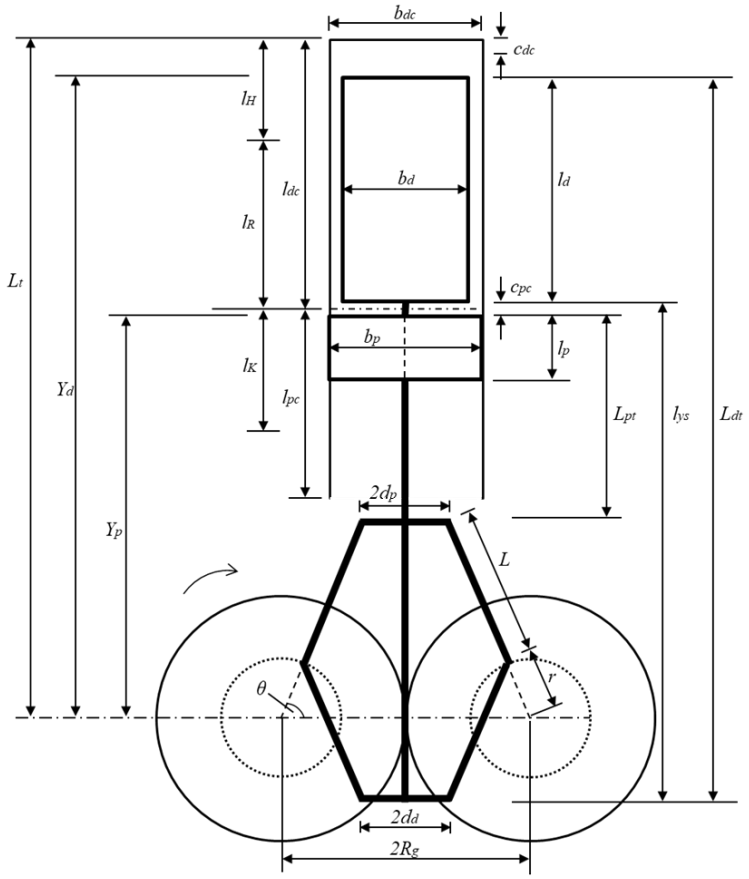

Figure 2. Schematic diagram of rhombic drive beta configuration Stirling engine

Table 1. Geometrical parameters of the Rhombic Drive Beta Configuration Stirling Engine

Components	**Label**	**Dimension (mm)**
Total length	L_t	416
Displacer top clearance	c_{dc}	3
Displacer cylinder bore	b_{dc}	84
Displacer cylinder length	l_{dc}	200
Displacer piston bore	b_d	81
Displacer piston length	l_d	182
Effective length of heater	l_H	48
Effective length of regenerator	l_R	152
Effective length of cooler	l_K	97.21
Power piston top clearance	c_{pc}	2.316
Power piston cylinder length	l_{pc}	144
Power piston bore (effective length)	b_p	80
Power piston length	l_p	50
Total length of displacer	L_{dt}	444
Total length of power piston	L_{pt}	200
Displacer yoke shaft	l_{ys}	262
Power piston yoke	$2d_p$	50
Displacer yoke	$2d_d$	50
Connecting rod length	$L_p=L_d=L$	80.5
Crank offset radius	r	38
Spur gear pitch diameter	$2R_g$	130

Source: (Farid et al., 2019)

The reciprocating displacements of the displacer, Y_d, and the reciprocating displacements of the power piston, Y_p, may be determined using the following relationships based on Figure 2. and the geometrical characteristics stated in Table 1.

$$Y_d = L_{dt} + r\sin\theta - \sqrt{L^2 - \left(R_g - d_d - r\cos\theta\right)^2} \quad (1)$$

$$Y_p = L_{pt} + r\sin\theta + \sqrt{L^2 - \left(R_g - d_d - r\cos\theta\right)^2} \quad (2)$$

The reciprocating volumetric displacement for expansion space is expressed as,

$$V_{SWE} = \pi\left(\frac{{b_d}^2}{4}\right)(L_t - c_{dc} - Y_d) \quad (3)$$

Meanwhile, the reciprocating volumetric displacement of the compression space is calculated using the displacement between the bottom surface of the displacer piston and the top surface of the power piston. The equation is expressed as follows,

$$V_{SWC} = \pi\left(\frac{{b_d}^2}{4}\right)\left(Y_d - l_d - Y_p - c_{pc}\right) \quad (4)$$

Based on Fig. 2, The heater volume in the heating zone is expressed as based on the equations of expansion and compression space sweeping volumes, as well as the geometrical characteristics described in Table 1.

$$V_H = \left(\frac{\pi}{4}\right)(b_{dc} - b_d)^2 l_H \quad (5)$$

Meanwhile, the regenerator space volume in the regenerating zone is written as,

$$V_R = \left(\frac{\pi}{4}\right)(b_{dc} - b_d)^2 l_R \quad (6)$$

For cooling zone volumes, the cooler volume is written as,

$$V_K = \left(\frac{\pi}{4}\right)\left(b_p - b_d\right)^2 l_K \quad (7)$$

Meanwhile, for rhombic drive principles, the engine stroke (power piston stroke is equal to length of cooler, l_K) follows that,

$$S = \left(\frac{r}{\lambda}\right)\left(\sqrt{(1+\lambda)^2 - \lambda^2\varepsilon^2} - \sqrt{(1-\lambda)^2 - \lambda^2\varepsilon^2}\right) \quad (8)$$

$$\lambda = \frac{r}{L} \quad (9)$$

$$\varepsilon = \frac{e}{r} \quad (10)$$

WORKING FLUID PROPERTIES

The Stirling Engine uses three main working fluids: air, hydrogen, and helium. To the best of our knowledge, working fluids for Stirling engines have been conducted in a variety of ways over the last decade, including the 3He component of the 3He-4He mixture to provide cooling at low temperatures below 2 K, hydrogen, atmospheric air, pressurized air, helium, strong real gas effects, such as CO2, HFC-125, HFC-23, ethane, and sodium (Chen et al., 2012). In contrast, changing the working fluid from air to hydrogen, for example, may enhance the power of the Stirling engine tenfold (Cheng et al., 2013).

NANOFLUID AND MATERIAL PREPARATION

In this current study, as for the alternative working fluid optimization study, the CuO-ZnO were applied. From the thermal properties studied refer Table 2 and Table 3, both experiment and numerically were conducted (Balla et al., 2012) for base fluid (f) are referred.

Table 2. Properties of Nanofluids at 30 °C. (Balla et al., 2012)

Nanofluid	Volume fraction (%)	Density (kg/m^3)	Specific heat (J/kg K)
CuO-water	0.2	1,011	4,133
	0.4	1,022	4,087.2
	0.6	1,033	4,042.31
	0.8	1,044	3,998.34
	1	1,064	3,892.54
ZnO-water	0.2	1,009.2	4,101.7
	0.4	1,018.4	4,098.9
	0.6	1,027.6	4,059.5
	0.8	1,036.8	4,020.7
	1	1,046	3,982.7
1CuO/2ZnO-water	0.2	1,009.8	4,102.2
	0.4	1,019.4	4,096.7
	0.6	1,029.4	4,055.1
	0.8	1,039.2	4,015
	1	1,049	3,975.7
2CuO/1ZnO	0.2	1,010.4	4,134.64
	0.4	1,020.8	4,090.2
	0.6	1,031.2	4,046.68
	0.8	1,041.8	4,003.24
	1	1,052	3,962.2

Table 3. Properties of Nanoparticle materials

Nanoparticles	Mean diameter (nm)	Density (kg/m^3)	Thermal conductivity (W/m K)	Specific heat (J/kg K)
CuO	50	6,500	17.65	533
ZnO	50	5,600	13	495

NANOFLUID MATERIAL PREPARATION

The calculation of the effective density ρ_{eff} and the effective specific heat $C_{p,eff}$ of a nanofluid from (Wang & Mujumdar, n.d.), is as stated in the equation 3.47 & 4.48. And to obtain the thermal conductivity of nanofluids is by applying the eq. 3.

$$\frac{k_{eff}}{k_f} = \frac{k_p + 2k_f - 2\varphi(k_f - k_p)}{k_p + 2k_f - 2\varphi(k_f - k_p)} \tag{11}$$

$$\rho_{eff} = \left(\frac{m}{V}\right)_{eff} = \frac{m_b + m_p}{V_b + V_p} = \frac{\rho_b V_b + \rho_p V_p}{V_b + V_p} = \left(1 - \phi_p\right)\rho_b + \phi_p \rho_b) \tag{12}$$

$$C_{\mathrm{p},eff} = \frac{\left(1 - \phi_p\right)\left(\rho C_p\right)_b + \phi_p\left(\rho C_p\right)_p}{\left(1 - \phi_p\right)\rho_b + \phi_p \rho_p} \tag{13}$$

BOUNDARY OPERATING CONDITIONS FOR THERMODYNAMIC NUMERICAL EVALUATION OF BCSE

From the Table 4., the proposed boundary condition is by applying almost identical with previous research by Farid et al. (2019) as for this paper is the continuation study to contributes toward maximum assumption for the BCSE working condition and design parameters.

Table 4. Boundary operating conditions for theoretical thermodynamic cycle evaluation

Parameters	**Input**
Heater Temperature (Kelvin)	1073.15
Cooler Temperature (Kelvin)	294.15
Working Fluid Charge Pressure (Bar)	4.5
Engine Speed (RPM)	300
Phase Angle (Degree)	90

RESULTS

As for the numerical model, similar Engine Configuration and boundary conditions were applied by Farid et al. (2019) using Helium as a working fluid and the experimental study by General Motors GPU-3 adapted the Helium and Hydrogen as working fluid (Rhombic-GPU-3, n.d.) were compared to the current thermodynamic prediction model (Refer Fig. 4). It can be seen that the present result is well agreed with the previous numerical model. However, the Experimental study for GPU-3 Beta Stirling Engine has a slight discrepancy on the P-V area diagram which is the rounded is smaller for the experimental, which means that less net work produced per cycle as the area enclosed is smaller.

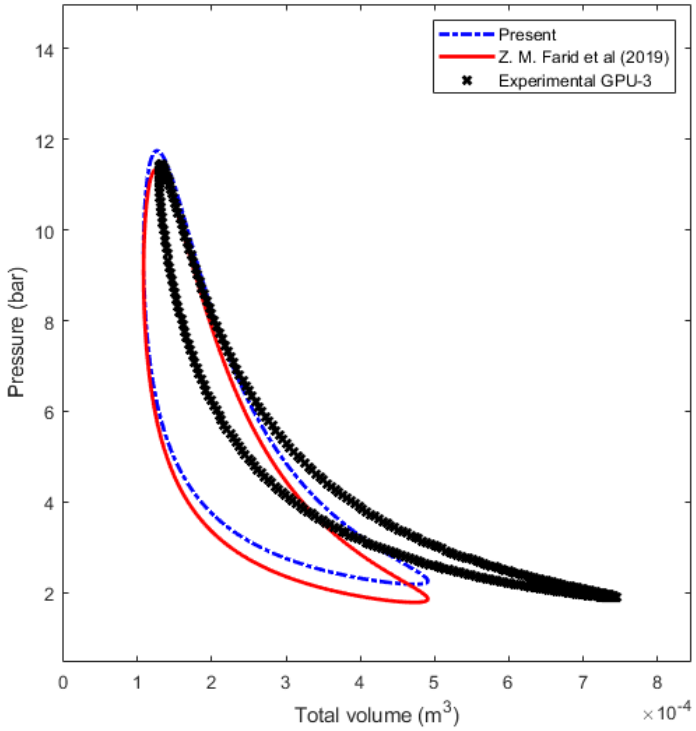

Figure 3. Validation on PV diagram data at (300 RPM,T_h=893 K, T_k=303 K, P = 4.5 Bar)

And from Fig. 4, based on the P-V diagram, the expansion space of the engine with the current thermodynamic model prediction is compared with other numerical methods applied as well as experimental. From Farid et al. (2019) by Schmidt Model, and (Yang & Cheng, 2017) used the Non-ideal Adiabatic model. It can be found that the experimental

is slightly high on the contraction stroke of the expansion space compared to the numerical. In addition, it can be noticed that the Non-ideal Adiabatic slightly has the expansion behaviors per cycle of the engine.

For the validation result of the various numerical analysis method compared in Fig. 5, found that all the model data according to the literatures studied is well agreed. For (Yang & Cheng, 2017) Non-Ideal Adiabatic and (Snyman et al., 2008) Simple Analysis, Ideal-Adiabatic, and Shmidt Model. It Can be observed that Simple Analysis and Non-ideal are closest to the experimental study.

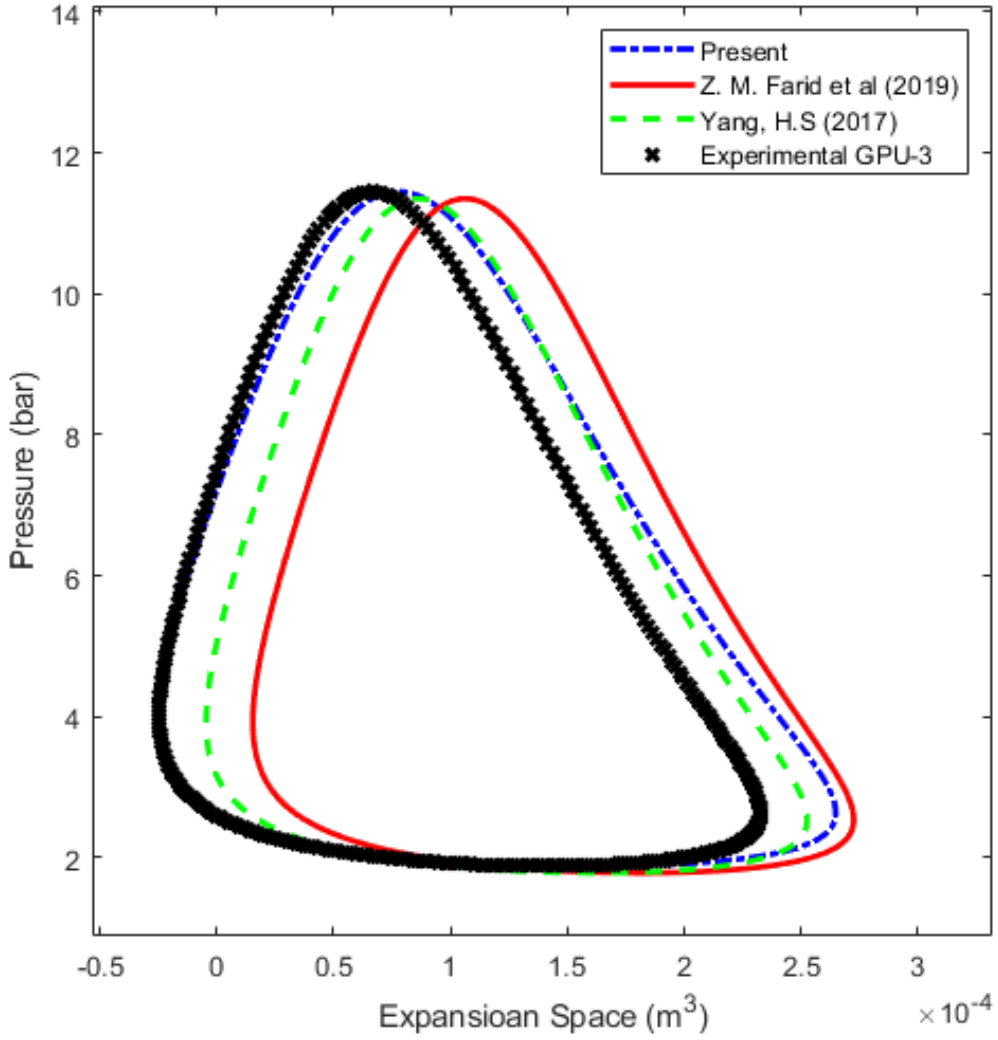

Figure 4. Pressure versus Expansion space by current and previous researchers.

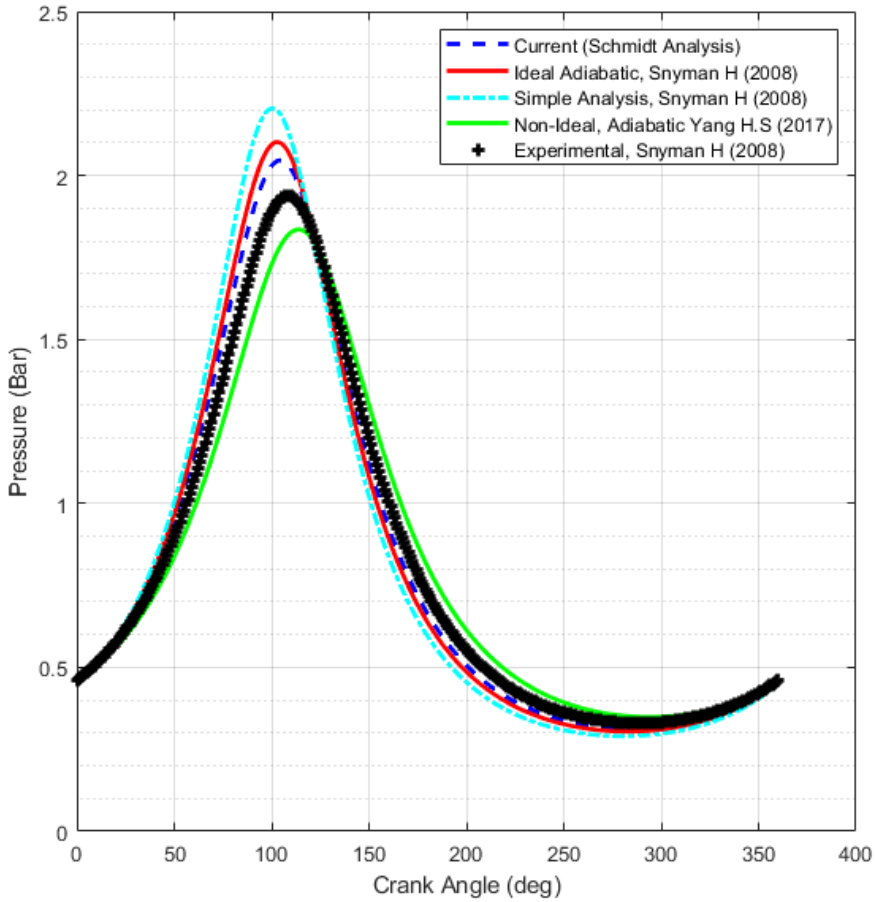

Figure 5. Pressure versus Crank Angle by current and previous researchers.

OVERALL ENGINE PERFORMANCE RESULTS

Table 5. Overall Thermodynamic performance analysis result of Rhombic-Drive Beta Configuration Stirling Engine.

Parameters	**Result Simulation**
Maximum pressure in cylinder (bar)	12.23
Minimum pressure in cylinder (bar)	1.66
Expansion swept volume (m^3)	4.1489e-04
Compression swept volume (m^3)	4.0285e-04
Heater volume (m3)	3.3929e-07
Regenerator volume (m3)	1.0744e-06
Cooler volume (m3)	7.6349e-08
Power (Watts)	946.54
Thermal efficiency (%)	72.59
Carnot efficiency (%)	72.59

Table 5 shown the overall performance results of Rhombic-Drive Beta Configuration Stirling Engine analysis by using CuO-ZnO as working fluids. Within this thermodynamic model, the engine parameter is similar to the previous research conducted by Farid et al. (2019) in Table 1. Considering that, this is the continuity research on Beta Configuration Stirling Engine optimizations to get maximum power output and the best condition parameters medium & lower power Engine application.

From the proposed designated working condition coupled with CuO-ZnO as working fluid, the maximum generating power is 946.59 watts at 300 RPM. The indicated Thermal Efficiency is calculated to be 72.59 % with a heat source temperature is 1073.15 K and a

cooler temperature of 294.15 K. Total mass of working fluid distributed between the compression, expansion and dead spaces remains constant. However, the engine performance as mentioned in (Kurt et al., 2018), (Petkar et al., 2020), and (Farid et al., 2019), the increase in the heater and cooler temperature difference decrease in the dead volumes will increase thermal efficiency and the pressurization method could increase the thermal energy absorption and rejection thus enhancing the engine performance are found to be perfectly match up. Increasing the heat of the temperature, increase the temperature of the working fluid in the hot zone area and hence the temperature difference between it and the cold zone, which produces an increase in performance. As for the real application of the Stirling Engine, to increase the heat source to the heater zone is by increasing heat in the burning room area. And the cooler temperature the method to vary in the cold zone area in the Engine is by varying the cooling water flow system or making the pipe water cool bigger since it was impossible to control vary the temperature because of running circulation water. Also found in this research, the geometric parameters of dead volume design are not affected in this 1st order analysis which is the opposite finding found by the experimental study by Finkelstein and Walker and Kahn 1965.

Figure 6 shows the engine's volumetric displacement for simulation based on the rhombic drive mechanism. In the simulation model, we assumed the displacer to be at TDC at a 90-degree crank angle. When heated, the volume in the expansion space increases while the volume in the compression area decreases to a minimum because there is minimal clearance between the displacer and the piston. The volume of the expanding space reaches its maximum within a short period of time when the displacer reaches BDC at a 270-degree crank angle and starts to decrease while the compression volume in the compression space is increased. As the displacer moves back to the TDC, the volume of the expansion space starts to decrease and resulting in the compression volume in the compression space reaching its maximum at a 360-degree crank angle.

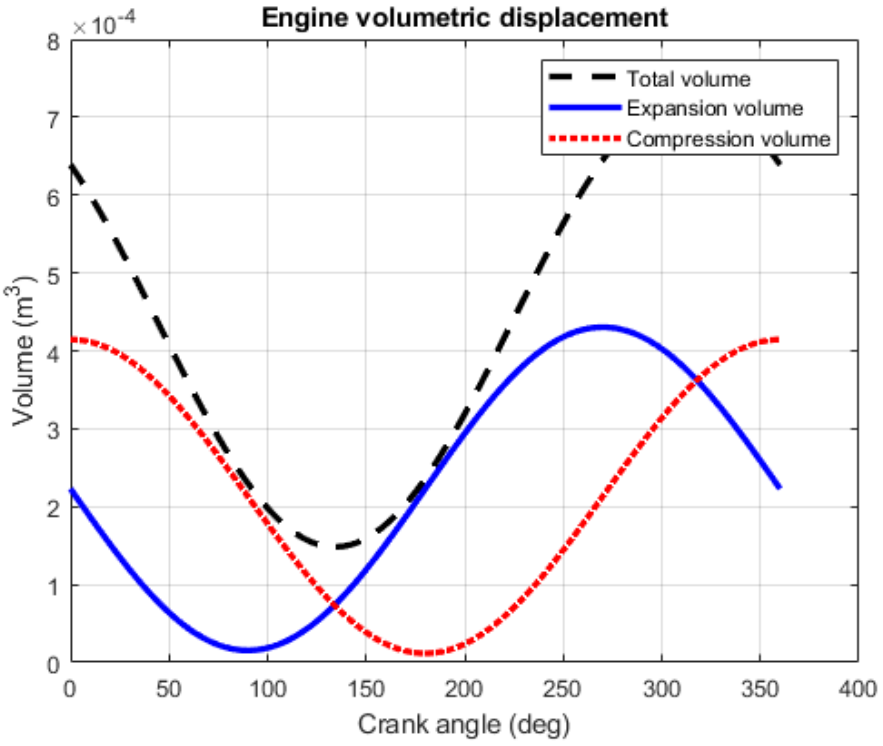

Figure 6. Engine volumetric displacement at (300 RPM, $T_h = 1073.15\,K$, $T_k = 294.15\,K$, P= 4.5 Bar, *WF* = CuO-ZnO).

The variation in the working fluid cycle pressure of the engine is shown in Fig. 7 (a). The engine's volumetric displacement is also shown to indicate the interaction between engine volume and pressure within the total volume. The fluid pressure inside the cylinder is fixed

constant at 4.5 bar for this simulation. Based on the heat source temperature of 1073.15 K at expansion space and cooling temperature of 294.15 K at compression space, the pressure varies from 1.66 bar to 12.23 bar.

For the volumetric displacement shown in Fig. 7 (b) the working fluid pressure reaches its maximum as the engine total volume reaches its minimum. The pressure is then decreased as both the displacer and power piston moving to BDC and resulting in an increment of expansion volume. When the displacer moves towards BDC, the displacer then compresses the working fluid in compressing space where at that particular time the power piston is at about TDC which results in compression volume inside the engine.

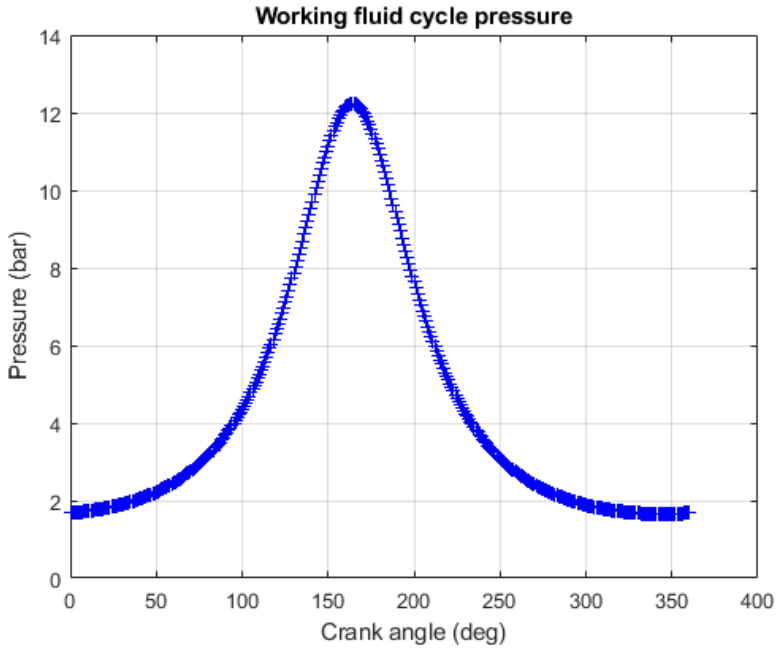

a. Working fluid cycle pressure

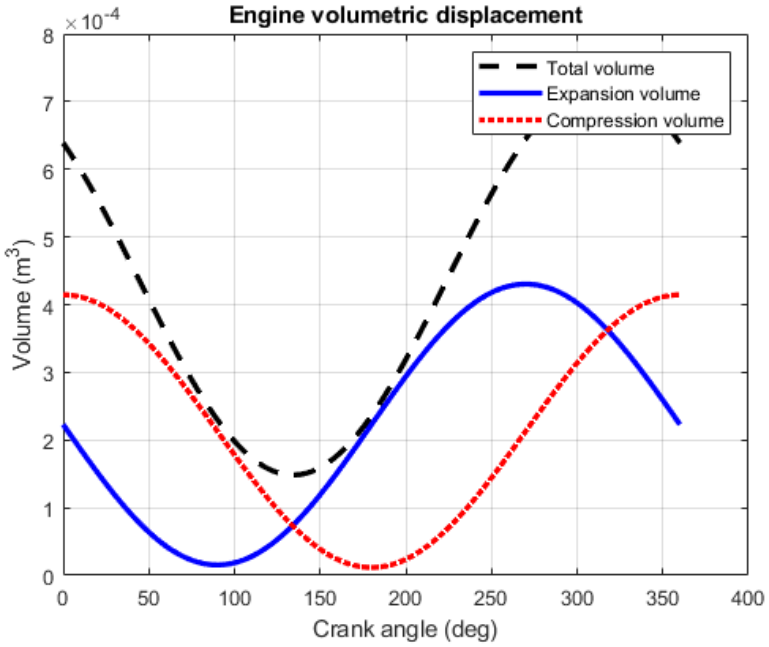

b. Engine volumetric displacement

Figure 7. Variation of working fluid cycle pressure and the Engine volumetric displacement at (300 RPM, $T_h = 1073.15\ K$, $T_k = 294.15\ K$, P = 4.5 Bar, *WF* = CuO-ZnO).

Meanwhile, the P-V diagram for the engine is shown in Figure 8. The area of the total volume diagram is said to be the output design criterion [28]. This means that a larger area of the total volume diagram indicates better engine performance. As from the P-V result obtained, the design parameters are generating good performance. During an adiabatic process no heat is transferred to the gas, but the pressure, volume, and temperature of the gas change. The total volume plotted, as the piston from the top around 12.23 bars goes down during the heat addition process, the volume of the system increases due to isothermal heat addition. Before it reaches the BDC, the isochoric heating removal process has occurred. Both the temperature and pressure of the system decrease due to the isochoric phase. After that, the isothermal heat removal process is starting, and the piston moves upward which is the compression process hence pressure of the system increases and volume decreases. When the pressure is around 6 bar the isochoric heat addition is taking place until reaches its maximum displacer top clearance.

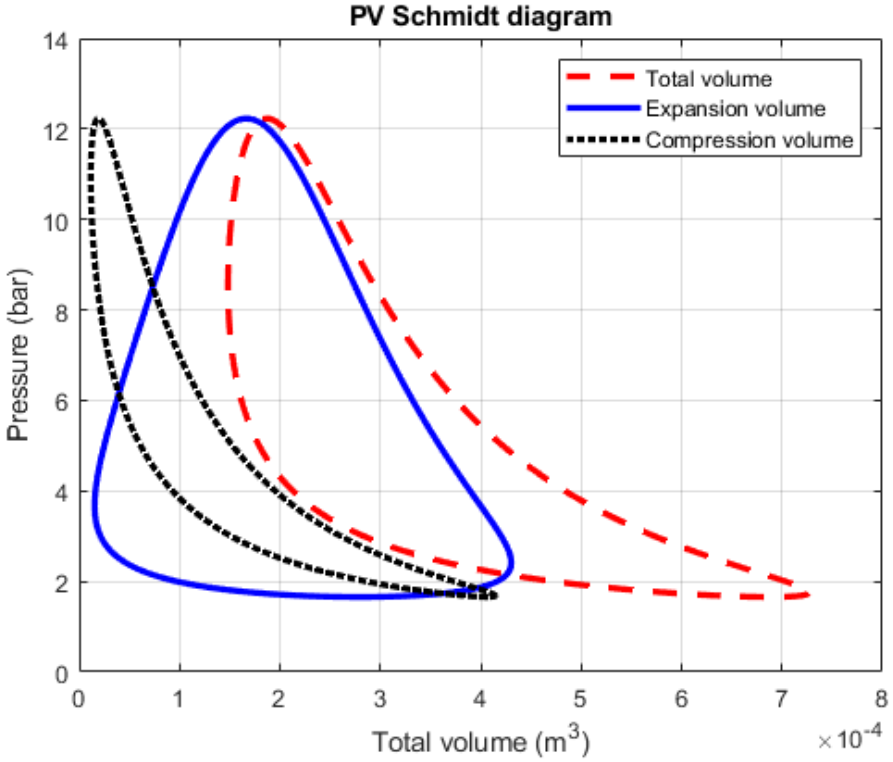

Figure 8. P-V diagrams of the rhombic drive BCSE at (300 RPM, $T_h = 1073.15\ K$, $T_k = 294.15\ K$, P = 4.5 Bar, *WF* = CuO-ZnO).

The variation of cyclic energy flow within expansion and compression space in the engine is shown in Fig. 9. The net amount of the heat energy which remained in the hot zone (expansion space) was transferred to the cold zone (compression space) through the regenerator in the hot flow. At the same time, the heat was ejected by the cooler in the cold zone (compression space). During the heating of the displacer cylinder's outer surface, higher thermal energy was absorbed from the expansion space and higher energy was rejected to the compression space within the engine cycle, thus increasing the total energy output [10]. According to Figure 4.5, the work produced during the crank rotation from 90-degree to 200-degree crank angle.

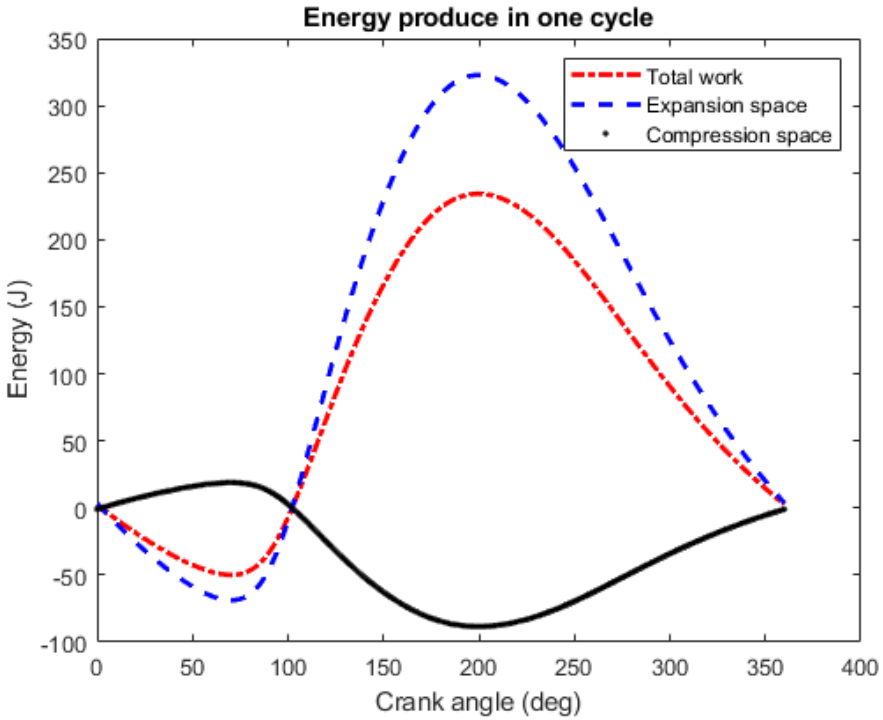

Figure 9. Cyclic energy flow within each engine space

Figure 10 shows the influence of engine power output at various phase angle settings. The increase in engine phase angle setting results in considerable differences in engine power output. This is one approach for managing the engine's output power. With a zero-phase angle, the volumes of compression and expansion change perfectly in phase, as if there were no cyclic flow of fluid through the system. The power control accomplished by adjusting the phase angle offers an immediate reaction and is an excellent approach for quick motor power control. Tested in this study at four different phase angle setting A (0˚, 360˚), B (90˚), C (180˚), and D (270˚). Found out at position A, the maximum change in volume without generating power. At position B, maximum power is generated. While the C setting variation of void volume and not generating power output. The last one at angle D found out maximum power absorption occurred, the piston acts as a brake.

Figure 11 depicts the influence of the engine's power output and thermal efficiency at various heat source temperatures. The results reveal that increasing the heat source temperature increased engine power production because more thermal energy contributed to the engine working space volumes, resulting in greater overall energy output. Similarly, the engine's thermal efficiency increases when the heat source temperature rises owing to a greater temperature differential between the expansion and compression spaces. Therefore, the results show that the rise in engine power output and thermal efficiency with heat source temperature is infinite, dependent on the use of sophisticated materials that are resistant to high-temperature heat sources (Çınar et al., 2018).

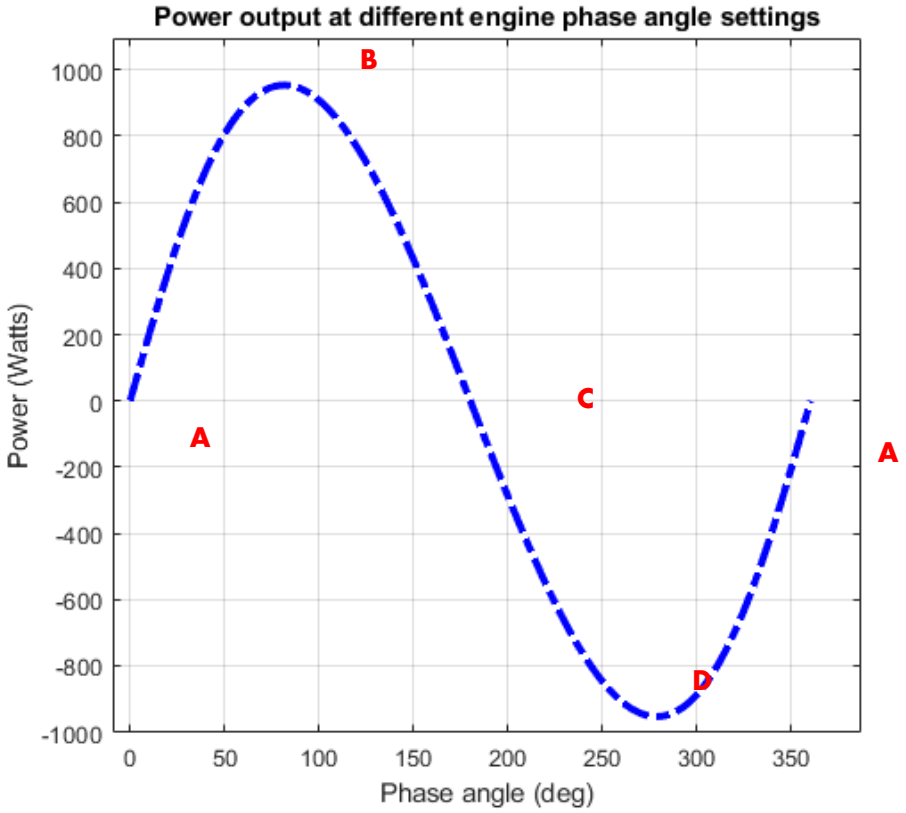

Figure 10. Effect of engine's power at different engine phase angle settings

Figure 12 shows the influence of varied working fluid charge pressures on engine power. The results reveal that the power output of the rhombic drive BCSE is directly related to the working fluid charge pressure. Because of the increased working fluid mass, increases in working fluid charge pressure improved engine power output. Increases in working fluid mass resulted in improved heat transfer and higher thermal energy absorption from the expansion space, as well as more energy rejection to the compression area during the engine cycle, resulting in an increase in total energy production (Çınar et al., 2018). As a result, the power at 4.5 bars pressure charge the maximum generated power is 946.54 W, from previous research conducted numerically by (Farid et al., 2019) by using Helium as working fluid tested at similarly engine parameters, only the designated temperature in the heater and cooler temperature are modified, T_h=1073.15 K and T_k=294.15 K to match the working condition for nanofluid, found out to be an increase in power output about 89% from previous. In the theoretical perception, the power output is improving as expected due to the nanofluid properties and the fluid behavior during the engine operating in a cold and hot zone. Nanofluid is improved in terms of thermal conductivity, high heat capacity, and low viscosity since the CuO-ZnO composite has a nanometer size with an average of 15.99-20 nanometer and a smaller band gap for each particle.

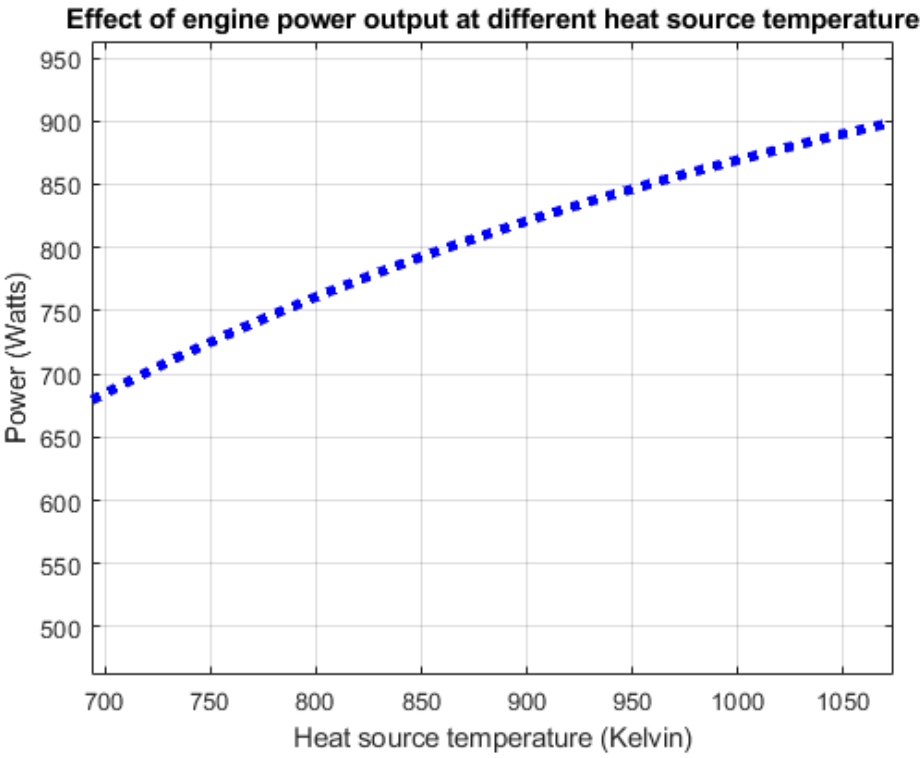

a. Engine power output

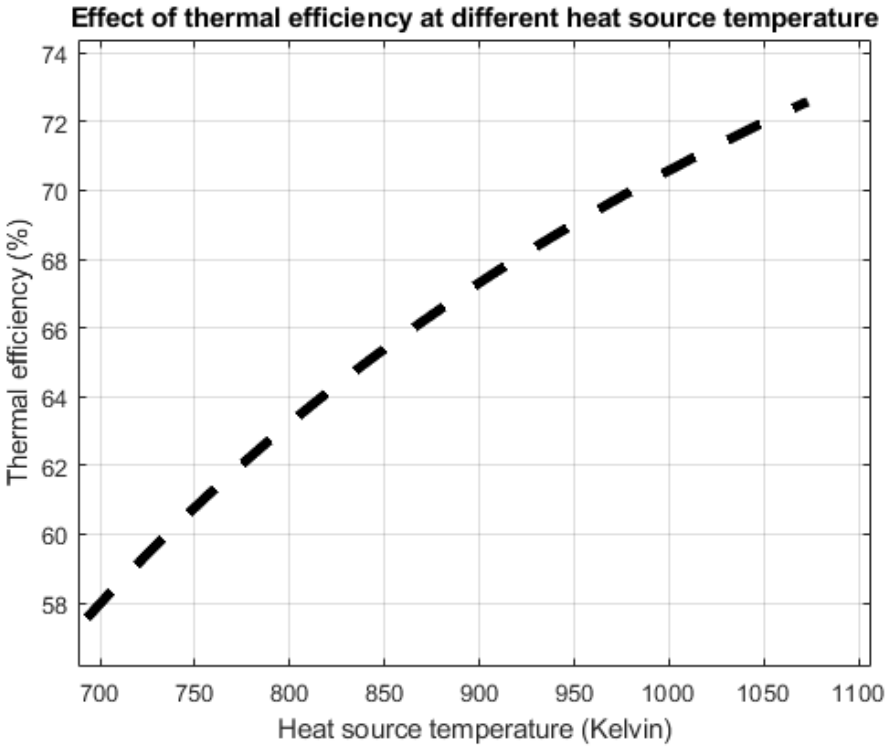

b. Thermal efficiency

Figure 11. Effect of engine's power output and thermal efficiency at different heat source temperature

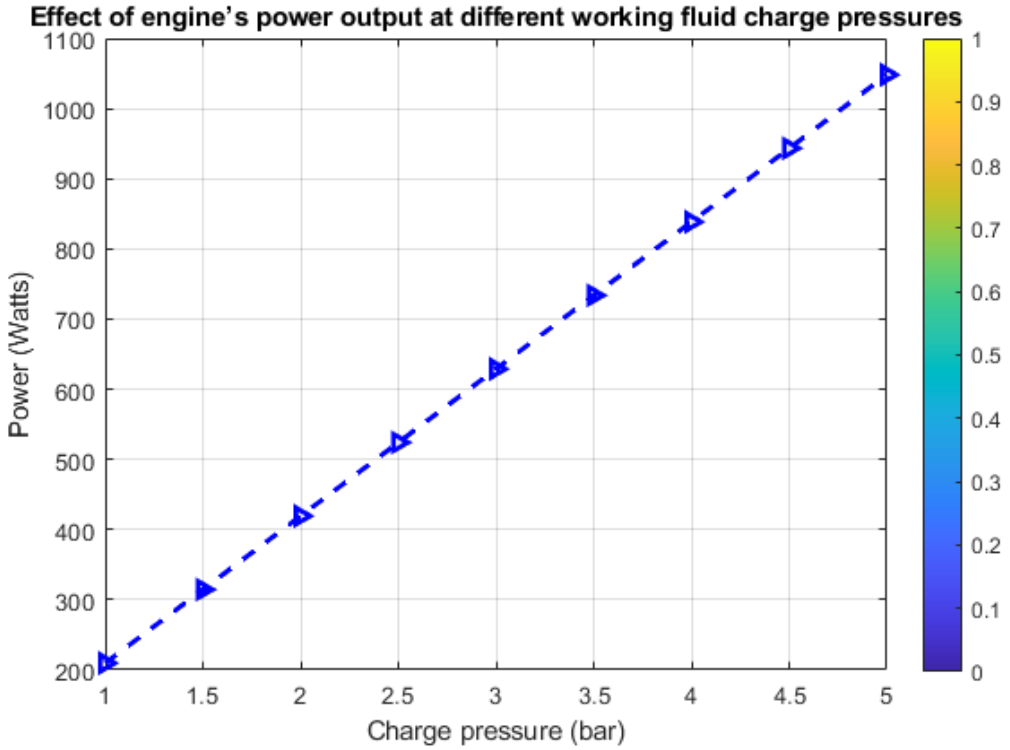

Figure 12. Effect of engine's power output at different working fluid charge pressure

CONCLUSION

The intended operating state and working fluid type are predicted. In the MATLAB environment, a thermodynamic simulation model for a rhombic drive beta configuration Stirling engine has been developed. This beta configuration Stirling engine was powered by a rhombic driving mechanism. Based on the rhombic drive Stirling engine, the prediction of reciprocating displacement, engine volumetric displacement, engine cycle, working fluid cycle pressure, cyclic energy flow, and effect of engine performance on different phase angles, charge pressure, engine speed, and temperature are presented and briefly discussed. From the thermodynamic model, the simulation has predicted the working fluid cyclic pressure in the engine to vary from 1.66 bar to 12.23 bar, and the engine's power output and indicated thermal efficiency of the rhombic drive BCSE are predicted to be 946.54 W and 72.59 % respectively by adapting the new alternative working fluid CuO-ZnO based on the designated working condition working fluid mean pressure of 4.5 bar, engine operating speed of 300 rpm, expansion space's temperature of 1073.15 K and cold space's temperature of 294.15 K. The alternative working fluid applied is CuO-ZnO, the thermal properties are adapted by employing the data from past research stud on the properties and Thermodynamic Chart Table is referred. The CuO-ZnO with enhanced performance such as the high thermal conductivity and heat capacity also low in viscosity and density since the sizing of CuO-ZnO is only around 15.99-20 nanometres and smaller band-gap for each particle. As mentioned previously by several researchers for working fluid performance studies using ZnO as a particle additive is enhance engine performance by 30%-40%. Found out that, the increase in power output by using CuO-ZnO as a working fluid is about 89% compared to Helium. Another conclusion that may be drawn is that, as predicted, the Schmidt Model (Carnot Efficiency) is larger than the single ideal-adiabatic, non-ideal-adiabatic, and nodal analyses. All of the thermodynamic models outperform the experimental data in the total comparative data. This is due, first and foremost, to the fact that numerous losses are not taken into account in most theoretical analyses, particularly for Schmidt and ideal-Adiabatic models (as we have already mentioned above). Furthermore, the combustion chamber losses, which could not be calculated exactly but were estimated, the flow resistance inside the engine,

and the pressure are not constant throughout the engine. The regeneration is not complete; there are heat losses in the regenerator. Furthermore, the expansion and compression are not adiabatic or isothermal; there is a heat drop across the heat exchanger surfaces. Above all, Stirling Engine is remaining a huge potential to be future affordable, efficient, silent, and most importantly clean energy for regeneration and prime movers' technology.

ACKNOWLEDGEMENTS

The authors would to thank Universiti Malaysia Pahang and the Faculty of FTKMA for providing all the needed facilities and resources for this research.

REFERENCES

Balla, H. H., Abdullah, S., Zulkifli, R., Faizal, W. M., & Sopian, K. (2012). Effect of oxides nanoparticle materials on the pressure loss and heat transfer of nanofluids in circular pipes. *Journal of Applied Sciences*, *12*(13), 1396–1401. https://doi.org/10.3923/jas.2012.1396.1401

Chen, W. L., Wong, K. L., & Po, L. W. (2012). A numerical analysis on the performance of a pressurized twin power piston gamma-type Stirling engine. *Energy Conversion and Management*, *62*, 84–92. https://doi.org/10.1016/j.enconman.2012.02.035

Cheng, C. H., Yang, H. S., & Keong, L. (2013). Theoretical and experimental study of a 300-W beta-type Stirling engine. *Energy*, *59*, 590–599. https://doi.org/10.1016/j.energy.2013.06.060

Çınar, C., Aksoy, F., Solmaz, H., Yılmaz, E., & Uyumaz, A. (2018). Manufacturing and testing of an A-type Stirling engine. *Applied Thermal Engineering*, *130*, 1373–1379. https://doi.org/10.1016/j.applthermaleng.2017.11.132

Farid, Z. M., Faiz, R. M., Rosli, A. B., & Kumaran, K. (2019). Thermodynamic performance prediction of rhombic-drive beta-configuration Stirling engine. *IOP Conference Series: Materials Science and Engineering*, *469*(1). https://doi.org/10.1088/1757-899X/469/1/012048

Kongtragool, B., & Wongwises, S. (2003). A review of solar-powered Stirling engines and low temperature differential Stirling engines. In *Renewable and Sustainable Energy Reviews* (Vol. 7, Issue 2, pp. 131–154). https://doi.org/10.1016/S1364-0321(02)00053-9

Kurt, E., Alaraby Ali Shufat, S., Mohamed El Hadad, K., & Hancerliogullari, A. (2018). A numerical model for a Stirling engine. *Journal of Energy Systems*, 1–1. https://doi.org/10.30521/jes.379164

Petkar, R., Society, Z. E., Sirsath, P., & Society, Z. E. (2020). *A Review on Stirling Engine Performance*. *April 2019*.

Snyman, H., Harms, T. M., & Strauss, J. M. (2008). Design analysis methods for Stirling engines. *Journal of Energy in Southern Africa*, *19*(3), 4–19. https://doi.org/10.17159/2413-3051/2008/v19i3a3329

Sripakagorn, A., & Srikam, C. (2011). Design and performance of a moderate temperature difference Stirling engine. *Renewable Energy*, *36*(6), 1728–1733. https://doi.org/10.1016/j.renene.2010.12.010

Thombare, D. G., & Verma, S. K. (2008). Technological development in the Stirling cycle engines. In *Renewable and Sustainable Energy Reviews* (Vol. 12, Issue 1, pp. 1–38). https://doi.org/10.1016/j.rser.2006.07.001

Tlili, I., Timoumi, Y., & Nasrallah, S. ben. (2008). Analysis and design consideration of mean temperature differential Stirling engine for solar application. *Renewable Energy*, *33*(8), 1911–1921. https://doi.org/10.1016/j.renene.2007.09.024

Urieli, I., & Berchowitz, D. (1984). Stirling Cycle Engine Analysis. In *Alternative Sources of Energy*.

Wang, X.-Q., & Mujumdar, A. S. (n.d.). *A REVIEW ON NANOFLUIDS-PART I: THEORETICAL AND NUMERICAL INVESTIGATIONS*. *25*(04), 613–630. www.abeq.org.br/bjche

Yang, H. S., & Cheng, C. H. (2017). Development of a beta-type Stirling engine with rhombic-drive mechanism using a modified non-ideal adiabatic model. *Applied Energy*, *200*, 62–72. https://doi.org/10.1016/j.apenergy.2017.05.075